

A Low-Power Dynamic-Range Relaxed Analog Front End for Wearable Heart Rate and Blood Oximetry Sensor

Hao Zhang, and Ye Li, *Member, IEEE*

Abstract—Photoplethysmogram(PPG) is widely implemented to monitor heart rate and oxygen saturation in wearable body sensor networks for healthcare management. This paper presents a low-power analog front end that enables PPG signal acquisition. By implementing a high-pass function, the AC and DC components of PPG signal are separately extracted to calculate heart rate and oxygen saturation, the dynamic range requirement of the readout channel is relaxed. Additionally, the chopping modulation is implemented to ensure the low-noise operation. The analog front-end circuit is designed and fabricated in CMOS 0.18- μm standard technology. The measurements show that the consuming power is approximately 180 μW at a supply of 2.5 V. The circuit achieves an input noise of 6.45 pA_{rms} . The calibrated algorithm is implemented using a Cortex-M3 MCU, and the demonstration, which is compared with the FLUKE Simulator as the reference, shows that the heart rate is accurately detected, and the error of the measured blood oxygen saturation is less than 1.5%.

Index Terms—analog front end, dynamic-range relaxed, chopping modulation, low power, photoplethysmogram.

I. INTRODUCTION

Body sensor networks(BSNs) have become the mainstream implementation for e-health systems because this smart approach meets the cost-effectiveness and convenience requirements of real-time health monitoring [1]–[3]. As a critical sensor node in BSNs, photoplethysmographic sensor capable of monitoring the important vital signs: heart rate(HR) and oxygen saturation (S_{PO_2}), is gaining increasing popularity in wearable BSNs-based applications. Furthermore, various PPG-based health monitoring implementations, such as blood pressure [4], [5], mental stress [6] and alertness [7], are proposed. The miniaturization and power consumption reduction in these sensor systems are realized as integrated circuit(IC) designs have proliferated [8]. Therefore, pulse oximetry, as a promising technique for measuring HR and S_{PO_2} [9], is usually implemented in IC technology. The implementation uses an infrared(IR) light source and a red(R) light source to illuminate the target object and a photodiode(PD) to capture the transmitted light. The analog front end(AFE) used

Manuscript received ; revised . The work is supported by National Natural Science Foundation of China: 61771465, Science and Technology Planning Project of Guangdong Province: 2015B010129012, Shenzhen Technological Research and Development Fund: CXZZ20150504145109589, J-CYJ20170413161515911, KQJSCX20170731165939298. (Corresponding author: Ye Li)

The authors are with Center for Biomedical Information Technology, Shenzhen Institutes of Advanced Technology, Chinese Academy of Sciences, Shenzhen 518055, China. (e-mail: ye.li@siat.ac.cn).

to implement the plus-oximeter system usually consists of two blocks: one is the transmitter(TX), which is the LED driver, and the receiver(RX), which comprises the PD and transimpedance amplifier(TIA). To save the chip power dissipation, the LEDs(IR and R) are usually pulsed at a fixed pulse repetition frequency(PRF). The produced PPG signal represents the light that has been absorbed by the finger and is divided in a DC component and an AC component. The AC-to-DC component ratio is minimal(typically 1%-4%). Hence, a receiver channel with a high dynamic range is usually required to enable the HR and S_{PO_2} measurements. The noise performance of the photodiode dc bias is also critical because its noise is directly injected at the input of the front-end receiver. Another issue in the RX design is the elimination of the ambient contribution in the DC component, which enables dynamic range(DR) enhancement.

To address these concerns, [10] consumes significant power to guarantee a sufficiently wide readout dynamic range for the processing of both AC and DC components, and a high-resolution $\Delta\Sigma$ -ADC is required. A high-pass function in TIA is performed through an error amplifier in the feedback to remove the ambient [11], which also eliminates the DC portion and is used for only the PPG measurements.

A logarithmic amplifier is implemented to increase the dynamic range [12], which increases design complexity. In [13], a reference voltage can subtract the average output of the TIA by using the feedback loop, which requires an ultra reference voltage circuit. Commonly, a current DAC in a digital feedback configuration is implemented in [14]–[17], Fig. 1 shows the basic concept: the static component(including the ambient and DC components of the PPG signal) is extracted and estimated in the MCU; then, a DAC controlled by the MCU generates a similar DC current to compensate the static component.

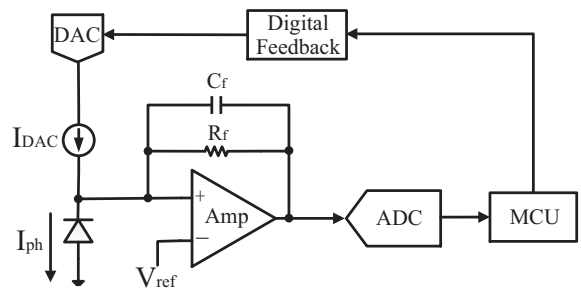


Fig. 1. Typical implementation for DR enhancement in RX.

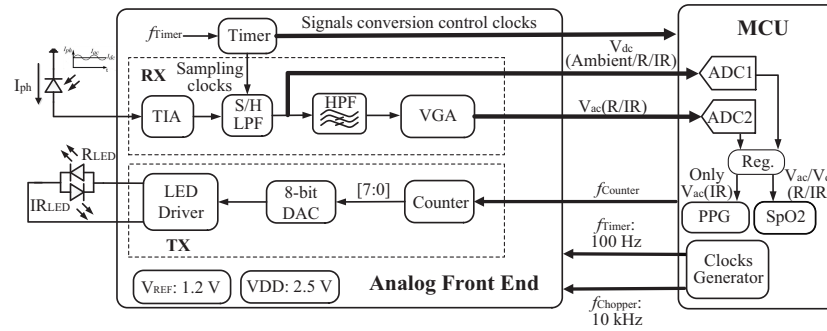


Fig. 2. System block diagram of the proposed pulse oximeter in this study.

Thus, large AC gains can be used without the large DC levels saturating the readout channel; then, the DR can be improved. However, the implementation complexity, size and power dissipation are added.

To solve these problems, a low-power plus-oximeter AFE is proposed in this work. First, the relaxation of the dynamic range requirement in RX is realized without using the DAC in the feedback implementation, which simplifies the design and saves both power and area consumption. The chopping technology is implemented to suppress the input noise. Second, an 8-bit LED driver capable of PPG signals acquisition is realized in TX circuit. Third, the control timing sequence implemented in this work enables the operation of AFE. Last but not least, HR and S_{PO_2} algorithms are calibrated to estimate the performance of AFE. The remainder of this paper is organized as follows: Section II presents the detail implementation of the proposed AFE. Section III provides the implemented HR and S_{PO_2} algorithms in our system. The measurements and demonstrations are illustrated in Section IV. Finally, Section V is the conclusion.

II. IMPLEMENTATION OF AFE

The implemented pulse oximeter system in this work is comprised of AFE, MCU, and LEDs, Fig. 2 shows the block diagram. The AFE mainly composed of RX channel and TX channel communicates with an external MCU. The MCU has the following functions: digitalizing and filtering the signals, controlling the LED driving current, and implementing the PPG extraction and S_{PO_2} calculation algorithms. Additionally, two clocks are generated: one for the chopping implementation($f_{Chopper}$), and the other for the timing sequence generation(f_{Timer}).

A. Receiver Channel

The proposed RX circuit shown in Fig. 2 consists of TIA, switched low-pass RC-filter, high-pass filter(HPF), and variable gain amplifier(VGA). Fig. 3 gives the detail implementation, the transfer function of TIA(for a high open-loop gain of amplifier) can be approximated as

$$V_O \approx \frac{I_{ph} R_F}{s R_F C_F + 1}, \quad (1)$$

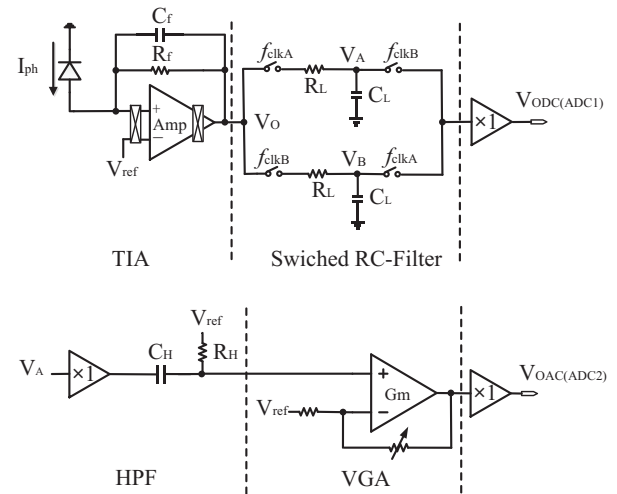


Fig. 3. Circuit implementation of the proposed RX.

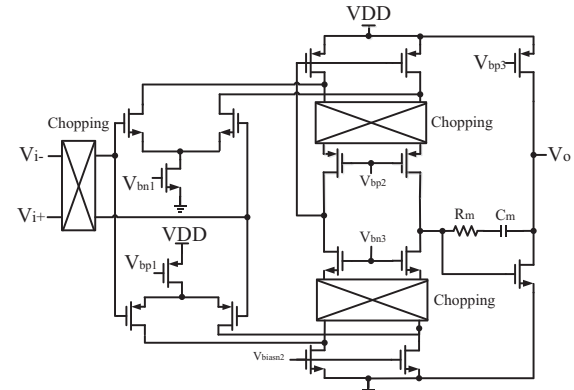


Fig. 4. Implemented amplifier in the TIA.

where I_{ph} is the PD current, s is the Laplace operator, R_f is the transimpedance gain, and C_f is the feedback capacitor. Considering the junction capacitance of the photodiode, the value of C_f should be carefully chosen to stabilize the TIA

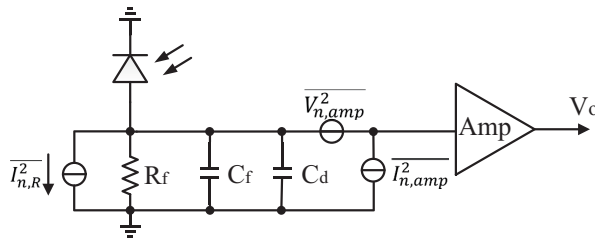


Fig. 5. Small-signal model for the noise analysis.

[18]. The main amplifier in the TIA has a two-stage fold-cascode structure [19], as shown in Fig. 4, the large open-loop gain of Amp ensures the accuracy of the TIA. Moreover, the differential input pairs that use both NMOS and PMOS transistors achieve a rail-to-rail input common-mode voltage range. Miller compensation, which is composed of capacitor C_m and resistor R_m , is implemented to ensure the stability.

One important feature of the TIA is its DR, which can be enhanced by increasing the sensitivity; i.e., the TIA must have less noise. A simplified small-signal model of TIA is used for the noise analysis, as shown in Fig. 5. C_d is the junction capacitance of the LED. The main noise sources are the thermal noise of R_f and the equivalent input noise sources of the amplifier $\overline{I_{n,amp}^2}$ and $\overline{V_{n,amp}^2}$. Then, the total input thermal noise current spectral density $\overline{I_{n,in}^2}$ can be calculated as [19]

$$\begin{aligned}\overline{I_{n,in}^2} &= \overline{I_{n,amp}^2} + \frac{\overline{V_{n,amp}^2} \cdot [1 + sC_t R_f]^2}{R_f^2} + \overline{I_{n,R}^2} \\ &\approx 4kT\gamma \frac{(2\pi f C_t)^2}{g_m} + \frac{4kT\gamma}{R_f^2 g_m} + \frac{4kT}{R_f},\end{aligned}\quad (2)$$

where k is Boltzmann's constant, $\gamma(= 2/3)$ is the white noise parameter for long transistors, $C_t = C_f + C_d$, and g_m is the transconductance of the MOS transistor. The thermal noise can be reduced by designing a large g_m . Thus, large input transistors are used in the Amp, which also decreases the flicker noise. Additionally, a chopping modulation is implemented in the amplifier to suppress the input noise and the input offset [20].

The photocurrent pulses from the PD are converted to a voltage using a TIA; then, it is demodulated using the switched RC low-pass filter. The low-pass corner can be given by [17]

$$f_{-3dB} = \frac{D}{2\pi R_L C_L}. \quad (3)$$

where D is the duty cycle of the sampling pulse. Thus, the filter cutoff can be controlled by adjusting the width of the sampling pulse to further reduce any noise aliasing that occurs at the output of the TIA.

Using the clock modulation, the TIA realizes two outputs: V_A and V_B . V_A includes both the LED(R and IR) light signal and the ambient light signal, whereas V_B is only the sampled ambient light signal; the separation is realized using

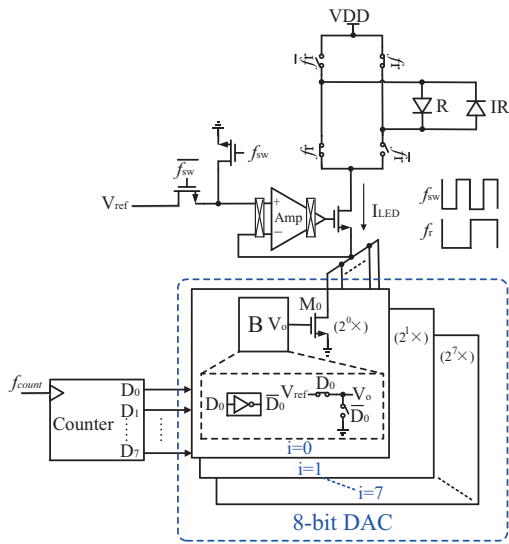


Fig. 6. Circuit implementation of TX.

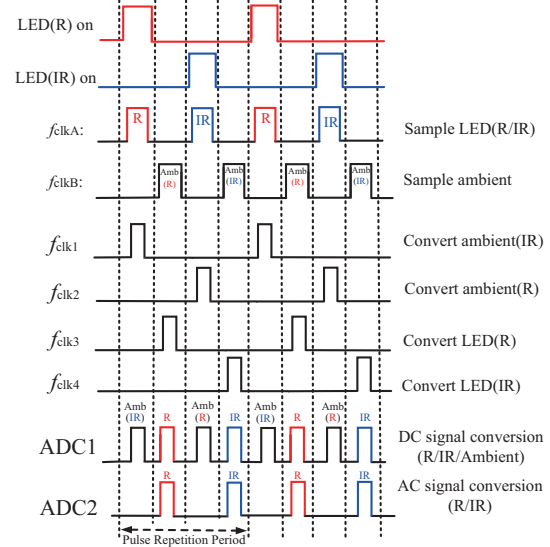


Fig. 7. Timer program implemented in the AFE.

the switched operation. Note that V_A is connected to an RC-filter that performs the high-pass function and blocks the DC signal, and that the values of C_H and R_H determine the cut-off frequency. Then, the baseline wander is removed, and the AC component of PPG signal is coupled to the VGA, which is implemented with a non-inverting architecture; the output swing of the VGA must satisfy only the gained AC signal requirement. In this way, the AC and DC portions of the PPG signal are separated by a high-pass structure, and then converted by ADC1 and ADC2, respectively. This operation relaxes the DR requirement of the RX channel.

B. Transmitter Channel

From Fig. 2, an LED driver that can drive dual LEDs is controlled by an 8-bit DAC and a counter to the MCU,

which can adjust different LED currents. The diagram of the proposed TX circuit is presented in Fig. 6. Based on the H-Bridge structure [10], the LEDs can be alternately driven through the operation of the clocks f_r and f_{sw} , and the duty cycle of the LED can be adjusted by changing the duty cycle of f_{sw} . To optimize the noise power performance of the driver output current, the differential pair of the two-stage fold cascode op-amp is chopped to remove the low-frequency noise. The LED current I_{LED} can be programmable using an 8-bit DAC and an 8-bit counter, which is controlled by the clock $f_{counter}$. The binary-weighted current sink transistors $M_{i(i=0 \sim 7)}$ are used for the 8-bit DAC implementation. The gate-source voltage of M_i is controlled by the logical unit B. When digital input bit $D_{i(i=0 \sim 7)}$ equals 1, the gate-source voltage is connected to V_{ref} , M_i is operated at the saturation region for the current generation. When D_i equals 0, the transistor turns off. Then, I_{LED} is expressed as

$$I_{LED} = \sum_{i=0}^7 D_i 2^i \mu_n C_{ox} \left(\frac{W}{L} \right) (V_{ref} - V_{th})^2, \quad (4)$$

where μ_n is the electron mobility, C_{ox} is the oxide capacitance per unit area, W/L is the size of transistor, and V_{th} is the threshold voltage. I_{LED} can be programmable by choosing different digital bits, the maximum value of I_{LED} is 50 mA.

C. Timer Module

Fig. 7 illustrates the operation of the timing control in the AFE, all timing sequences are non-overlapping operations and generated by the timer circuit, f_{clkA} and f_{clkB} are implemented to sample the LED signals and ambient light signals, respectively. With the operation, the sampled LED and ambient signals are alternatively sent to the MCU, as shown in Fig. 3. Since the two different LED signals(I and IR) are alternatively generated, clocks f_{clk1} and f_{clk2} (f_{clk3} and f_{clk4}), which are used as the control signals for the ADC1 and ADC2 operations, are implemented to control the converting process of two different ambient signals(LED signals). This operation also ensures that all converted data can be correctly collected and stored in the MCU.

III. HR AND SPO_2 ALGORITHMS

HR is obtained by using the frequency of AC signal and can be expressed as [5]

$$BPM = Frequency_{AC} \times 60. \quad (5)$$

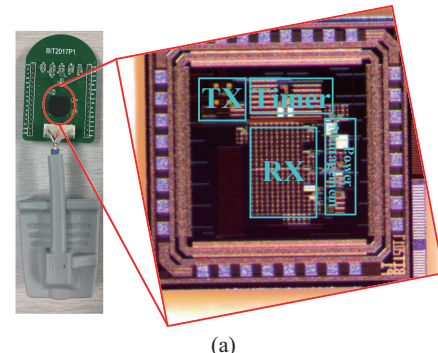
SPO_2 can be calculated according to absorption ratio R, which is expressed as [9]

$$R = \frac{\ln(AC_R/DC_R)}{\ln(AC_{IR}/DC_{IR})}. \quad (6)$$

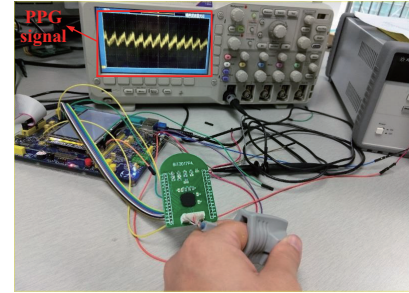
Then, SPO_2 can be described as a linear function [5]:

$$SPO_2 = A \cdot R + B, \quad (7)$$

where A and B are experimental calibration coefficients. To determine the relationship between R and SPO_2 , the values of A and B are derived according to curve-fitting data from several various PPG signals. Then, the accurate algorithm of SPO_2 detection can be obtained.



(a)



(b)

Fig. 8. Proposed AFE:(a) chip micrograph; (b) demonstration of PPG measurement.

IV. MEASUREMENTS AND DEMONSTRATIONS

The proposed AFE circuit is implemented in the CMOS 0.18- μ m process. Fig. 8(a) shows the chip diagram of the proposed AFE, and external LEDs are used. An off-chip C_H of 2 nF is selected to achieve a high-pass cutoff frequency of 0.5 Hz in this work, and the signal bandwidth is set to 10 Hz. Fig. 8(b) demonstrates the measured original PPG waveforms of the real subject with our proposed AFE.

Fig. 9(a) presents the test setup that estimates the performance of our proposed AFE to monitor HR and SPO_2 . The FLUKE Simulator is used to provide the PPG signals for the monitor, and a calibrated algorithm is implemented using the Cortex-M3 MCU(STM32). The measured values(HR and SPO_2) are displayed using an LCD. The framework for implementing the test setup is shown in Fig. 9(b), the performance of our AFE is demonstrated and estimated by comparing the measured HR and SPO_2 with the input signal from the FLUKE Simulator. LEDs are modulated by a frequency of 100 Hz, and the duty cycle is set to approximately 25%. Fig. 10 illustrates the output waveforms of AFE, which also demonstrates the dynamic DC cancellation by using a high-pass filter. V_A is the discrete PPG signal, and V_{OAC} is the amplified AC component that is separate from V_A . Both the DC and AC signals, as the inputs, are connected to the MCU, where two 12-bit SAR ADCs are used to convert the different signals. Fig. 11 shows the operational performance in the MCU, in which the AC and DC components of different PPG signals are extracted.

To determine the SPO_2 -R relationship described in Section III, the FLUKE Simulator is used for the calibration, the value

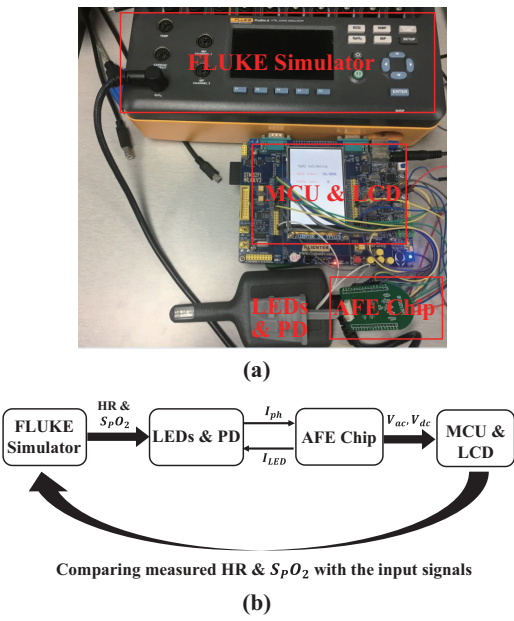


Fig. 9. (a) Test setup for the proposed AFE; (b) framework implementation of test setup.

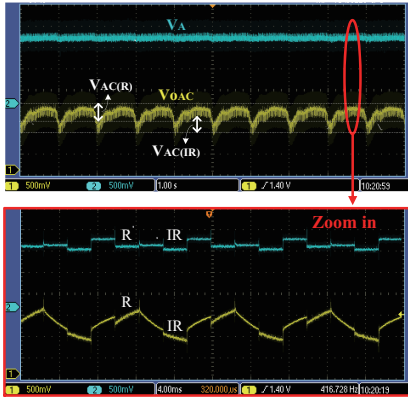


Fig. 10. Experimental output waveforms of the AFE.

of R measured using our AFE is recorded according to the input S_pO_2 value generated from the FLUKE Simulator. The experiment is implemented on five values of S_pO_2 (80%, 85%, 90%, 95%, 100%), each point is tested in 10 samples, and the mean of R is obtained. With the collected curve-fitting data, the exact linear function shown in Eq. (7) can be plotted.

After calibrating our pulse oximeter, we measure HR and S_pO_2 , and the results are compared with those generated from the FLUKE Simulator. Fig. 12 shows the measured performance, each data point reflects the average of five tests at each target, and each test is implemented for 30 seconds. Fig. 12(a) provides the measured HR when the input frequency of the PPG signal is swept within 0.67-2.5 Hz. Fig. 12(b) presents the S_pO_2 measurements, where the maximum standard error is less than 1.5%.

The experimental input current noise density is shown in Fig. 13, with the chopping modulation, the integrated value is

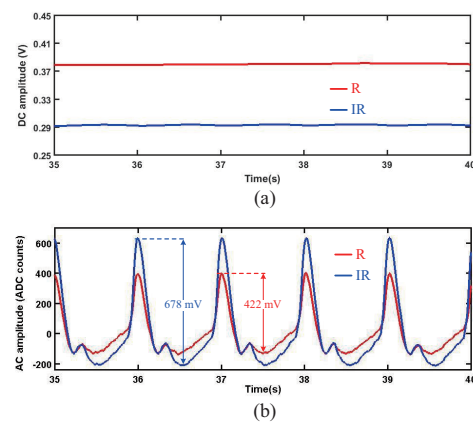


Fig. 11. Calculated PPG signals in MCU:(a) DC portion; (b) AC portion.

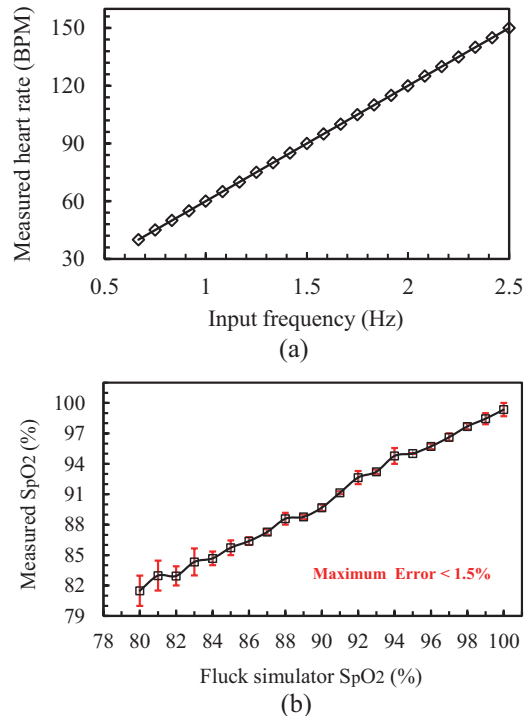


Fig. 12. Demonstrated results:(a) heart rate; (b) S_pO_2 .

approximately 6.45 pA(0.5-10 Hz).

Table I summarizes the characteristics of our AFE compared with those of published state-of-the art systems. The comparison reveals that the proposed AFE enables HR and S_pO_2 monitoring, the implementation eliminates the dynamic DC component of the PPG signal without the additional DAC in the feedback operation that is implemented in [10], [14], [16], [17]. While [11]–[13] also implement HR and S_pO_2 measurements without DAC implementation, but they consume more power dissipation. The proposed circuit performs better in terms of power consumption. Moreover, the chopping modulation ensures the circuit performs low input noise with the low transimpedance gain($= 40 \text{ k}\Omega$).

TABLE I
COMPARISON WITH OTHER STATE-OF-THE-ART AFES FOR PPG ACQUISITION.

	This work	Ref. [10]	Ref. [11]	Ref. [12]	Ref. [13]	Ref. [14]	Ref. [16]	Ref. [17]
Process	0.18 μm	0.18 μm	0.35 μm	1.5 μm	0.35 μm	0.18 μm	0.18 μm	0.13 μm
Supply voltage (V) ^a	2.5	3.3	2.5	5	3.3	1.8	1.2	1.5
Power (μW) ^a	180	1980 ^b	600 ^b	400	363	216 ^c	171.6 ^c	68.7 ^c
Integrated noise (pA_{rms})	6.45	3.2	2200	N/A	890	600	486	4
Bandwidth (Hz)	10	20	6		10	10	10	5
Sampling frequency (Hz)	100	100	100	100	100	165	128	100
R_f (Ω)	40k	500k	2k	N/A	500k	1M	50k	100k
LED peak current (mA)	50	100	N/A	15	7.1	25.6	0.036	50
LED duty cycle	25%	25%	10%	3%	4%	0.7%	N/A	20%
DAC implementation for dynamic DC cancellation	No	Yes	No	No	No	Yes	Yes	Yes
Application	HR & SPO_2	HR & SPO_2	HR	SPO_2	HR & SPO_2	HR & SPO_2	HR	HR

^a Exclude LED and power management.

^b Only RX.

^c Include ADC.

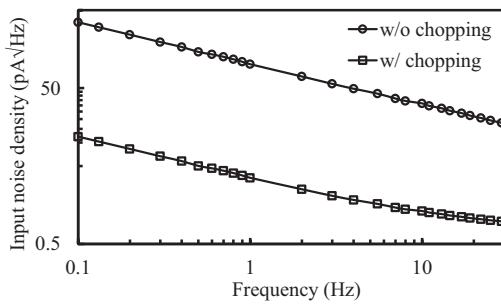


Fig. 13. Experimental input noise density.

V. CONCLUSION

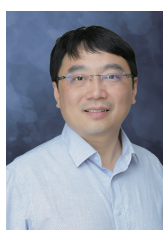
In this work, a low-power AFE is implemented for the PPG signals acquisition. With the high-pass operation, a simple solution to separate the DC and AC signals is realized. Consequently, the dynamic range burden of the AFE for the AC portion extraction is relaxed. Using a calibration implemented in the MCU, the proposed circuit has excellent performance in terms of HR and SPO_2 detection. The design can ensure a precise pulse oximeter front end for applications in wearable healthcare systems.

REFERENCES

- [1] A. Andreoli, R. Gravina, R. Giannantonio, P. Pierleoni, and G. Fortino, "SPINE-HRV: A BSN-based toolkit for heart rate variability analysis in the time-domain," *Lecture Notes in Electrical Engineering*, vol.75, pp.369–389, 2010.
- [2] G. Fortino, R. Giannantonio, R. Gravina, P. Kuryloski, and R. Jafari, "Enabling effective programming and flexible management of efficient body sensor network applications," *IEEE Transactions on Human-Machine Systems*, vol.43, no.1, pp.115–133, Jan. 2013.
- [3] R. Gravina, P. Alinia, H. Ghasebzadeh, and G. Fortino, "Multi-sensor fusion in body sensor networks: State-of-the-art and research challenges," *ELSEVIER Information Fusion*, vol.35, pp.68–80, May 2017.
- [4] G. Fortino and V. Giamp, "PPG-based methods for non invasive and continuous blood pressure measurement: an overview and development issues in body sensor networks," 2010 IEEE International Workshop on Medical Measurements and Applications, pp.10–13, April 2010.
- [5] J. Wannenburg and R. Malekian, "Body sensor network for mobile health monitoring, a diagnosis and anticipating system," *IEEE Sensors Journal*, vol.15, no.12, pp.6839–6852, Dec. 2015.
- [6] P.M. Mohan, V. Nagarajan, and S.R. Das, "Stress measurement from wearable photoplethysmographic sensor using heart rate variability data," 2016 International Conference on Communication and Signal Processing (ICCP), pp.1141–1144, April 2016.
- [7] J. Dey, T. Bhownik, S. Sahoo, and V.N. Tiwari, "Wearable PPG sensor based alertness scoring system," 2017 39th Annual International Conference of the IEEE Engineering in Medicine and Biology Society (EMBC), pp.2422–2425, July 2017.
- [8] B. Calhoun, J. Lach, J. Stankovic, D. Wentzloff, K. Whitehouse, A. Barth, J. Brown, Q. Li, S. Oh, N. Roberts, and Y. Zhang, "Body sensor networks: a holistic approach from silicon to users," *Proceedings of the IEEE*, vol.100, no.1, pp.91–106, Jan. 2012.
- [9] J. Webster, "Design of pulse oximeters," Bristol, PA, USA: Philadelphia: Institute of Physics Pub., 1997, Medical Science Series.
- [10] "Ultra-small, integrated analog front-end for heart rate monitors and low-cost pulse oximeters," TI AFE4403, Jul. 2014.
- [11] A.K.Y. Wong, K.P. Pun, Y.T. Zhang, and K.N. Leung, "A low-power CMOS front-end for photoplethysmographic signal acquisition with robust DC photocurrent rejection," *IEEE Trans. Biomed. Circuits Syst.*, vol.2, no.4, pp.280–288, Dec. 2008.
- [12] M. Tavakoli, L. Turicchia, and R. Sarapeshkar, "An ultra-low-power pulse oximeter implemented with an energy-efficient transimpedance amplifier," *IEEE Trans. Biomed. Circuits Syst.*, vol.4, no.1, pp.27–38, Feb. 2010.
- [13] K. Glaros and E. Drakakis, "A sub-mW fully-integrated pulse oximeter front-end," *IEEE Trans. Biomed. Circuits Syst.*, vol.7, no.3, pp.363–375, June 2013.
- [14] E.S. Winokur, T. O'Dwyer, and C.G. Sodini, "A low-power, dual-wavelength photoplethysmogram (PPG) SoC with static and time-varying interferer removal," *IEEE Trans. Biomed. Circuits Syst.*, vol.9, no.4, pp.581–589, Aug. 2015.
- [15] Y. Lee, H. Lee, J. Jang, J. Lee, M. Kim, J. Lee, H. Kim, K.R. Lee, K. Kim, H. Cho, S. Yoo, and H.J. Yoo, "A 141 uW sensor SoC on OLED/OPD substrate for SpO_2 /ExG monitoring sticker," 2016 IEEE International Solid-State Circuits Conference (ISSCC), pp.384–385, Jan. 2016.
- [16] P.V. Rajesh, J.M. Valero-Sarmiento, L. Yan, A. Bozkurt, C.V. Hoof, N.V. Helleputte, R.F. Yazicioglu, and M. Verhelst, "A 172 uW compressive sampling photoplethysmographic readout with embedded direct heart-rate and variability extraction from compressively sampled data," 2016 IEEE International Solid-State Circuits Conference (ISSCC), pp.386–387, Jan. 2016.
- [17] A. Sharma, A. Polley, S.B. Lee, S. Narayanan, W. Li, T. Sculley, and S. Ramaswamy, "A sub-60- μA multimodal smart biosensing SoC with >80-dB SNR, 35- μA photoplethysmography signal chain," *IEEE J. of Solid-State Circuits*, vol.52, no.4, pp.1021–1033, April 2017.
- [18] A. Bhat, "Stabilize your transimpedance amplifier," Maxim Application Note, pp.1–11, Feb. 2012.
- [19] T. Carusone, D. Johns, and K. Martin, "Analog Integrated Circuit Design," Wiley, 2011.
- [20] C. Enz and G. Temes, "Circuit techniques for reducing the effects of op-amp imperfections: autozeroing, correlated double sampling, and chopper stabilization," *Proceedings of the IEEE*, vol.84, no.11, pp.1584–1614, Nov. 1996.



Hao Zhang received B.E. and M.E. in Microelectronics from Lanzhou University, Lanzhou, China in 2007 and 2010, respectively. He received the Ph.D degree in the Graduate school of Information, Production and System, Waseda University, Fukuoka, Japan. He is now an assistant researcher in the Center for Biomedical Information Technology, Shenzhen Institutes of Advanced Technology, Chinese Academy of Sciences. His research interests are low-power analog integrated circuits and biomedical circuits.



Ye Li is a Professor in Shenzhen Institutes of Advanced Technology (SIAT), Chinese Academy of Sciences. He received the B.S. and M.S. degrees in electrical engineering from University of Electronic Science and Technology of China, Chengdu, China, in 1999 and 2002, respectively. In 2006, he received the Ph. D. degree in electrical engineering from Arizona State University, AZ, U.S. Since 2008, he is the Director of Research Center for Biomedical Information Technology in SIAT. His current research interests include wireless body sensor networks, wearable devices and mobile health etc.